RSC Advances

PAPER

View Article Online
View Journal | View Issue

Open Access Article. Published on 22 April 2020. Downloaded on 10/31/2025 4:51:06 PM.
This article is licensed under a Creative Commons Attribution-NonCommercial 3.0 Unported Licence.

Check for updates

Cite this: *RSC Adv.*, 2020, **10**, 15901

Degradation of *p*-nitrophenol by nano-pyrite catalyzed Fenton reaction with enhanced peroxide utilization†

Tong Liu,[ab] Nan Chen,[b] Yang Deng,[b] Fangxin Chen[b] and Chuanping Feng*[ab]

Received 6th February 2020
Accepted 9th April 2020

DOI: 10.1039/d0ra01177k

rsc.li/rsc-advances

Pyrite (FeS_2) catalyzed conversion of H_2O_2 into oxidants is increasingly recognized as a promising Fenton-like process for treating recalcitrant contaminants. However, the underlying mechanism remains unclear, especially for nano-pyrite. The present study explored the potential of a nano-pyrite Fenton system for *p*-nitrophenol oxidation using high energy ball milled nano-pyrite. The enhancement in $^{\bullet}OH$ production, with 3 times faster *p*-nitrophenol degradation than the conventional Fenton system, is ascribed to the reduction of pyrite size to the nanoscale, which alters the Fe^{2+} regeneration pathway, favoring faster and very efficient production of $^{\bullet}OH$ during H_2O_2 decomposition. The amount of H_2O_2 required was reduced due to the increased conversion efficiency of H_2O_2 to $^{\bullet}OH$ from 13.90% (conventional Fenton) to 67.55%, in which surface S_2^{2-} species served as an electron source. An interpretation of the degradation intermediates and mineralization pathway of *p*-nitrophenol was then made using gas chromatography-mass spectrometry. This study bridges the knowledge gap between *p*-nitrophenol removal and the nano-pyrite catalyzed oxidant generation process.

1. Introduction

Advanced oxidation processes (AOPs) are widely regarded as a potential approach to treat various refractory contaminants.[1] High redox potential radicals produced in AOPs (such as hydroxyl radicals, sulfate radicals, and superoxide radicals) can attack pollutants unselectively.[2,3] Among all AOPs, the Fenton reaction, employing H_2O_2 and Fe^{2+} to produce $^{\bullet}OH$, has been studied extensively and is considered promising for organic wastewater treatment owing to its high efficiency, simplicity, non-toxicity, and cost-effectiveness.[4] However, there are some inherent drawbacks of the conventional Fenton reaction, such as narrow operating pH range, a large volume of iron sludge produced, an excessive amount of Fe^{2+} required, and possible corrosion of the equipment.[5,6] These disadvantages, along with poor cost-effectiveness under high pollution load, still impair the widespread application of the Fenton reaction.[7]

In the past decades, continuous efforts have been made to optimize the overall efficiency of Fenton reaction, for example, by employing heterogeneous catalysts instead of soluble iron salts.[4] Using heterogeneous catalysts has many advantages including wide operating pH range, extended catalyst life, and easy separation.[8] In heterogeneous Fenton reaction, natural minerals with special crystal properties have been studied as promising alternative catalysts.[9] And the most catalysts used were iron-bearing minerals, such as schorl, goethite, hematite, pyrite, and magnetite.[10]

Among these minerals, pyrite (FeS_2), one of the most abundant iron sulfide mineral in earth's crust and a common industrial waste,[11] showed high catalytic activities because of its high iron content, specific surface area (SSA), and porosity.[12] Using micro-pyrite Fenton system, complete degradation of diclofenac was achieved within 120 s,[13] and an 80% removal of nitrobenzene was accomplished.[14] Other researchers have demonstrated successful degradation of TCE,[15] 2,4,6-trinitrotoluene,[16] and pyrene[17] using micro-pyrite Fenton system. Nevertheless, still, some demerits limited the application of micro-pyrite Fenton, such as a deficient dispersion and a large catalyst dosage needed due to its high density (~5 g cm^{-3}), which can result in augment in investment and operation cost. The utilization of nano-pyrite in heterogeneous Fenton-like system could resolve these two aforementioned challenging issues and has achieved efficient removal of acid orange 7 (96.30%) with lower H_2O_2 concentration (5 mM) and pyrite dosage (0.5 g L^{-1}) compared to the use of micro-pyrite.[18] The enhancement of micro-pyrite Fenton reaction compared to conventional Fenton reaction was ascribed to the self-regulation of pH and continuous release of Fe^{2+} ion.[13,15,17,19] However, limited information has been provided to explain the observed high efficiency in nano-pyrite Fenton reaction. It is

[a]MOE Key Laboratory of Groundwater Circulation and Evolution, China University of Geosciences (Beijing), No. 29 Xueyuan Road, Haidian District, Beijing 100083, P. R. China. E-mail: fengcp@cugb.edu.cn; Fax: +86-10-82322281; Tel: +86-10-82322281

[b]School of Water Resources and Environment, China University of Geosciences (Beijing), No. 29 Xueyuan Road, Haidian District, Beijing 100083, P. R. China

† Electronic supplementary information (ESI) available: Supporting information available. See DOI: 10.1039/d0ra01177k

Open Access Article. Published on 22 April 2020. Downloaded on 10/31/2025 4:51:06 PM.
This article is licensed under a Creative Commons Attribution-NonCommercial 3.0 Unported Licence.

therefore of great economic and environmental interest to further investigate the ˙OH generation mechanism in nano-pyrite Fenton reaction.

To fulfill this knowledge gap, we investigated thoroughly the potential of nano-pyrite Fenton system for *p*-NP oxidation, which was chosen as a model contaminant due to its high toxicity and ubiquitous existence in natural water bodies.[3,20,21] In this study, *p*-NP mineralization through a heterogeneous Fenton-like process catalyzed by nano-pyrite was characterized. Batch experiments were executed to investigate the degradation kinetics of *p*-NP in nano-pyrite catalyzed Fenton system, to evaluate the effects of key operating parameters (pyrite dosage, H_2O_2 concentration, and initial pH) on the removal kinetics of *p*-NP, and to identify the degradation mechanism.

2. Materials and methods

2.1 Chemicals and materials

p-NP (>99%), H_2O_2 (30 wt%) were purchased from Guangfu Fine Chemical Co., Ltd. (Tianjin, China). HPLC grade methanol was purchased from MREDA Co., Ltd. (Portland, US). Iso-propanol (2-propanol) (>99%) and chloroform (>99%) were purchased from Sinopharm Chemical Reagent Beijing Co., Ltd. (Beijing, China). *N*,*O*-Bis (trimethylsilyl) trifluoro-acetamide (BSTFA, ≥99.0%) was bought from Sigma-Aldrich. Deionized water (DIW) was used to prepare solutions. Natural pyrite minerals were collected from Qu Jing city (Yunnan, China).

2.2 Nano-pyrite preparation and characterization

Firstly, natural pyrite minerals were washed using 1 M HCl to remove the impurity, and crushed using a grinder (ZN-04, China) to reduce their size to μm scale. Then, the obtained pyrite powder was milled in a high energy planetary ball mill (QM3-SP04, China) at 400 rpm for 24 h to obtain nanosized particles. The mass ratio of ceramic milling ball to pyrite powder used was 10 : 1. Ethanol was selected as grinding aids (4 mL/5 g).[22] The as-milled powder was transferred into ethanol and treated with ultrasonic for 45 min to reduce the agglomeration.[23] Finally, the sample was freeze-dried in vacuum (FD-1A, Biocool, China). Characterization of nano-pyrite using SEM, XRD, FT-IR, XPS, and BET analyzer was stated in detail in the ESI.†

2.3 *p*-NP removal experiments

Experiments to investigate the degradation of *p*-NP by pyrite Fenton reaction were carried out in glass flasks containing 100 mL of reaction solution (initial *p*-NP concentration: 100 mg L^{-1}). For preparing reaction solution, 90 mL of pH adjusted (using 1 M HCl or NaOH) DIW containing pyrite particles (0.030 g) were treated with ultrasonic for 5 min to eliminate agglomeration of pyrite particles, and then mixed with 10.0 mL of *p*-NP stock solution (1.0 g L^{-1}). After stirring 30 min to achieve adsorption and desorption equilibrium, the degradation of *p*-NP by pyrite Fenton reaction was initiated by adding 3% H_2O_2 (306 μL) into the flask with an initial concentration of 3 mM. Three controls (*p*-NP + DIW, *p*-NP + DIW + pyrite, *p*-NP + DIW + H_2O_2) were prepared to evaluate possible losses of *p*-NP by volatilization, sorption on the wall of glass flask and pyrite surface, and oxidation by H_2O_2, respectively. Degradation of *p*-NP by classic Fenton system was also tested using Fe^{2+} solution of 10.0 mg L^{-1} at pH 4. All samples and controls were performed at least in duplicate.

At predetermined time intervals, 1 mL of reaction solution was transferred immediately into a 1.5 mL plastic centrifuge tube that contains 0.2 mL 2-propanol. The centrifuge tube was shaken using a Vortex (IKA MS3, Germany) to quench the reaction rapidly, and then centrifuged at 14 000 rpm for 10 min for pyrite particles separation. To further investigate the *p*-NP removal mechanism in nano-pyrite Fenton system, several experiments were conducted. Contribution from ˙OH and $^{\cdot}O_2^-$ was determined using iso-propanol as ˙OH scavenger due to its high reactivity with oxidants ($k_{\cdot OH,2\text{-propanol}} = 3 \times 10^9$ M^{-1} s^{-1}) but low reactivity with reductants ($k = 1 \times 10^6$ M^{-1} s^{-1}), and chloroform as a scavenger for $^{\cdot}O_2^-$ because of its high reactivity with reductants ($k = 3 \times 10^{10}$ M^{-1} s^{-1}) but low reactivity with oxidants ($k_{\cdot OH,chloroform} = 7 \times 10^6$ M^{-1} s^{-1}).[3] Besides, the concentrations of total aqueous Fe, aqueous Fe^{2+}, and aqueous Fe^{3+} were measured.

2.4 Analytical methods

The concentration of *p*-NP was determined using high-performance liquid chromatography (HPLC 1260, Agilent, US) obeying method depicted in ESI.† To clarify the effects of environmental parameters on *p*-NP degradation kinetics in the heterogeneous Fenton reaction, the experimental data obtained in the early stage were fitted using pseudo-first-order kinetics (eqn (S1)†), and their rate constants were calculated and compared. The concentrations of ferrous ion and total iron were measured with 1,10-phenanthroline following standard method at 510 nm using a UV/Vis spectrophotometer (UV-1800, Shimadzu, Japan). The electron spin resonance (ESR) experiment was conducted using MS-5000 spectrometer (Magnettech, Germany) and DMPO as ˙OH trapper with sweep width, microwave frequency, power set at 332.5–342.5 mT, 9.46 GHz, and 10 mW, respectively. The degradation intermediates of *p*-NP were analyzed using GC-MS (GC-2014, Shimadzu, Japan).

3. Results and discussion

3.1 Characterization of pyrite nanoparticles

The XRD reflection peaks for both pyrite nanoparticles before and after reaction at 2θ of 23.46°, 34.84°, 39.76°, 47.4°, 52.32°, 60.79°, 62.65°, and 68.9° could be indexed to the cubic phase of pyrite (JCPDS 00-042-1340), which also correspond to the crystal planes of (111), (200), (210), (211), (220), (311), (222), and (023), respectively[24] (Fig. 1(A)). The XRD data showed pyrite particles were of great crystallinity and structural stability during the planetary ball milling process,[18] and the average crystal size was calculated to be 68.5 ± 55.58 nm. Only peaks from pyrite were detected for particle sample after Fenton reaction, showing there was no iron sludge formed. However, these peaks showed a considerable reduction in height, implying the decrease of

Open Access Article. Published on 22 April 2020. Downloaded on 10/31/2025 4:51:06 PM.
This article is licensed under a Creative Commons Attribution-NonCommercial 3.0 Unported Licence.

crystallite size (58.9 nm), which was in consist with Diao *et al.*[25] A higher decrease in (200) and (311) surfaces of nano-pyrite was observed, these two surfaces were found to be S-rich surfaces among the fresh surfaces exposed during crush and grind processes.[26] The S atoms tend to catch O atom from water molecular, and sulfate was released as oxidized products under acidic atmosphere.[27] With the continuous loss of S atom, the (200) and (311) planes, as S-rich sites, therefore showed severe erosion than other planes of nano-pyrite.

To investigate the surface functional groups changes of nano-pyrite, FT-IR analysis was conducted (Fig. 1(B)). The wideband at 3410.6 cm^{-1} can be ascribed to the stretch vibration of the O–H group, the peaks at 1629.6 cm^{-1} indicated Fe–SO_4 species which was oxidized from FeS_2, and the peaks at 1140.1 and 1086.8 were due to the presence of Fe–OOH.[18] The small peaks below 1000 cm^{-1} were assigned to the stretching vibration of Fe–S. No new band was detected in the FT-IR spectrum of used nano-pyrite, indicating an unchanged pyrite surface, which further proved the catalyst stability.

The surface morphology of pyrite nanoparticles before and after Fenton reaction was determined by SEM. The illustrated distribution of highly uniform pyrite particles (Fig. 1(C) and (D)) corroborated the successful transformation of pyrite microparticles to nanoparticles using high energy planetary ball milling process. Compared to the SEM images of fresh nano-pyrite catalysts, the shapes of used nano-pyrite catalysts were much sharp, which was caused by the erosion of different lattice planes during the autocatalytic oxidation process.[28] The observed decrease of nano-pyrite particles from SEM images (Fig. 1(E) and (F)) was consistent with crystal size reduction calculated with XRD data. The prepared pyrite nanoparticles can be dispersed in polar solvents (Fig. 1(H)). It was found that the maximum fluoresce intensity showed at 400–450 nm while 3–10 nm pyrite particles were tested, and the wavelength increased with the increase of particle size.[24] The as made pyrite nanoparticles showed a maximum fluoresce intensity at 600 nm in our study, indicating a larger particle size than 10 nm (Fig. 1(I)), which was also confirmed with a medium size of ~75 nm given by size distribution data from laser sizer data (Fig. S1†).

3.2 Enhanced degradation of *p*-NP by pyrite nanoparticles catalyzed Fenton reaction

p-NP is a highly recalcitrant molecule and the decrease of *p*-NP concentrations in all controls can be neglected (Fig. 2(A)), indicating that *p*-NP losses by volatilization in batch reactor,

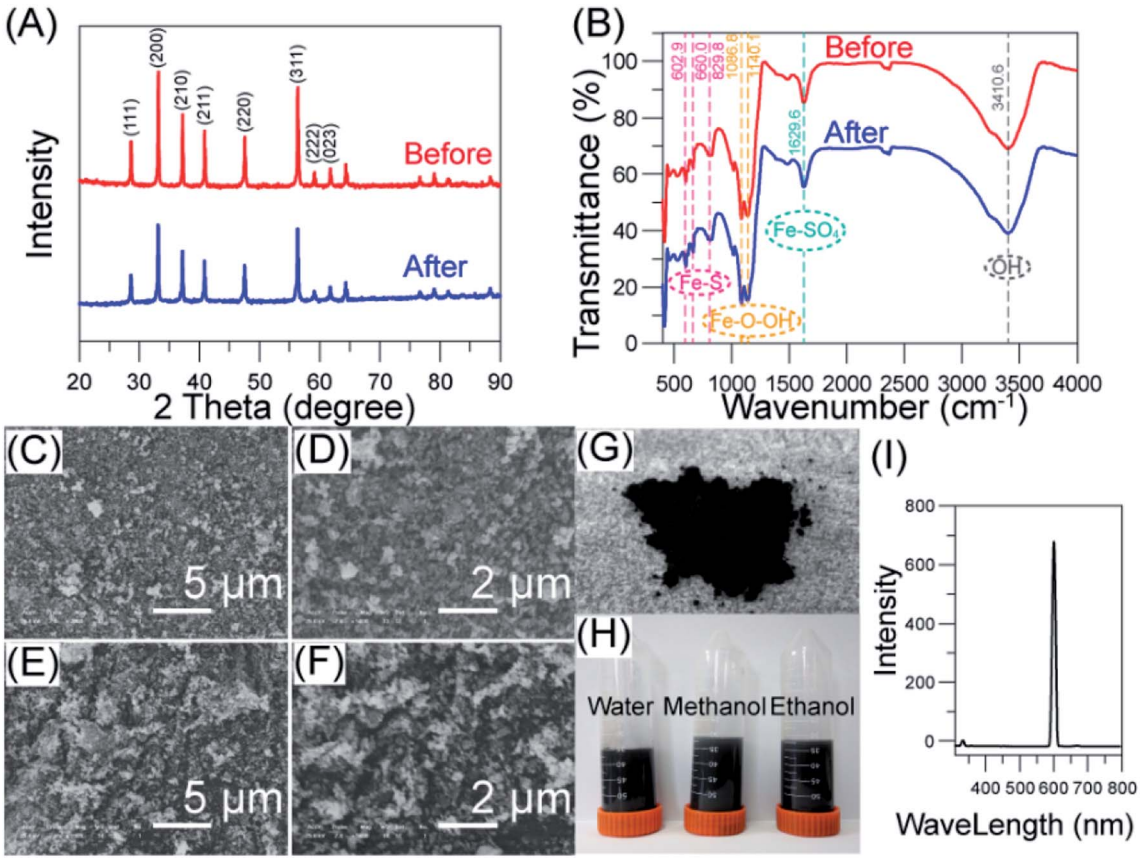

Fig. 1 Characteristics of the prepared nano-pyrite. XRD patterns (A) and FT-IR spectra (B) of nano-pyrite catalyst before and after pyrite Fenton reaction. SEM pics of pyrite nanoparticles before (C and D) and after reaction (E and F) at different magnification. Optical photograph of the prepared pyrite nanoparticles (G). Optical photographs of pyrite nanoparticles dispersed in different solvents (H). Fluoresce spectrum of pyrite nanoparticles dispersed in ultrapure water (25 °C) (I). The excitation wavelength for the fluorescence spectrum was 300 nm.

Open Access Article. Published on 22 April 2020. Downloaded on 10/31/2025 4:51:06 PM.
This article is licensed under a Creative Commons Attribution-NonCommercial 3.0 Unported Licence.

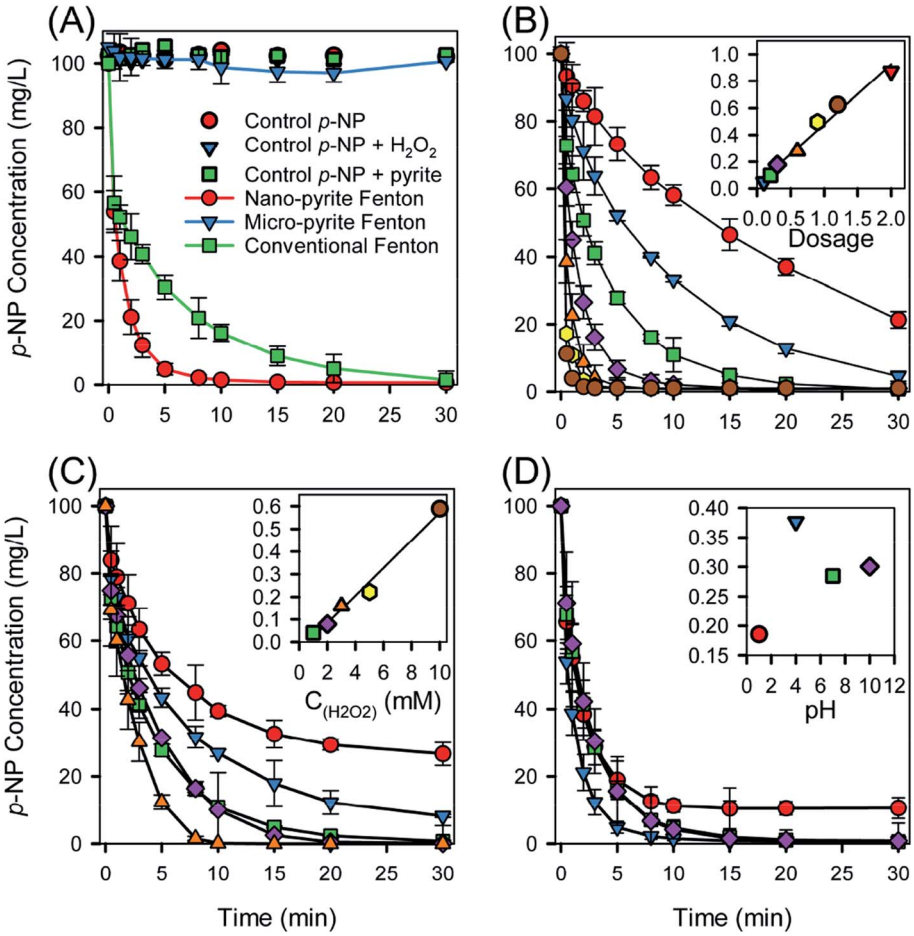

Fig. 2 (A) Comparison of ferrous iron and pyrite catalyzed Fenton reactions for the degradation of *p*-NP. Effects of (B) pyrite dosage, (C) H_2O_2 concentration, and (D) initial pH on the degradation of *p*-NP in the heterogeneous Fenton reaction. Environmental boundary conditions: $[p\text{-NP}]_0 = 100$ mg L^{-1}, initial pH = 4, pyrite dosage = 0.30 g L^{-1}, $[H_2O_2]_0 = 3.0$ mM, and temperature = 25 ± 0.5 °C.

sorption on pyrite surface and reactor, and direct oxidation by H_2O_2 were not significant. No *p*-NP degradation was observed in micro-pyrite catalyzed Fenton, in contrast, fast *p*-NP removal was achieved using nano-pyrite. This discrepancy was majorly due to difference in specific surface area (SSA), of which the SSA was 15.45 and 1.31 m^2 g^{-1} for pyrite nano and microparticles, respectively. The increase in SSA leads to an increment in catalytic capacity due to more active sites existed on the catalyst surface. The degradation of *p*-NP was fitted with pseudo-first-order rate equation, estimated rate constants were 0.3771 min^{-1} ($R^2 = 0.988$) and 0.1215 min^{-1} ($R^2 = 0.999$) for nano-pyrite Fenton and conventional Fenton, respectively. With the presence of both nano-pyrite and H_2O_2, *p*-NP degradation was progressively enhanced, of which the kinetics constant was 3 fold as great as that of conventional Fenton. Approximately, 99% of the *p*-NP was removed in pyrite Fenton reaction within 15 min, while 98% of *p*-NP was removed within 30 min in classic Fenton reaction. The difference in degradation rates was ascribed to the efficient regeneration of Fe^{2+} on the surface of nano-pyrite. The typical classic Fenton reaction contained two reactions (eqn (3) and (5)), the production of $^{\bullet}OH$ (eqn (3), $k_1 = 76$ M^{-1} s^{-1}) was limited by the low rate constant of Fe^{2+} regeneration (eqn (5), $k_2 = 0.01$–0.02 M^{-1} s^{-1}). However, Fe^{2+} was generated dominantly following (eqn (1) and (4)) in pyrite Fenton reaction. The rate expression associated with eqn (4) is eqn (6),[29] leading to a sufficient Fe^{2+} concentration.[30] It should also be noted that iron sludge formation (a key issue in classic Fenton) was not observed in nano-pyrite Fenton, which was in agreement with XRD data (Fig. 1(A)). The stoichiometric efficiency, defined as the amount of *p*-NP decomposed per mole of H_2O_2 consumed was used to compare the performance of catalysts.[31] The stoichiometric efficiency of the nano-pyrite catalyst was calculated to be 33%, was 825, 5.4, and 3.7 times greater than that of nano-magnetite (0.04%),[3] zero-valent iron with microwave irradiation (6.11%),[32] and saponin modified nano-magnetite (8.99%),[33] respectively.

$$2FeS_2 + 7O_2 + 2H_2O \rightarrow 2Fe^{2+} + 4SO_4^{2-} + 4H^+ \quad (1)$$

$$2FeS_2 + 15H_2O_2 \rightarrow 2Fe^{3+} + 14H_2O + 4SO_4^{2-} + 2H^+ \quad (2)$$

$$Fe^{2+} + H_2O_2 \rightarrow Fe^{3+} + {}^{\bullet}OH + OH^- \quad (3)$$

$$FeS_2 + 14Fe^{3+} + 8H_2O \rightarrow 15Fe^{2+} + 2SO_4^{2-} + 16H^+ \quad (4)$$

Open Access Article. Published on 22 April 2020. Downloaded on 10/31/2025 4:51:06 PM.
This article is licensed under a Creative Commons Attribution-NonCommercial 3.0 Unported Licence.

$$Fe^{3+} + H_2O_2 \rightarrow Fe^{2+} + {}^{\bullet}OOH + H^+ \quad (5)$$

$$\mathrm{Rate}(Fe^{3+}) = SA(m/m_0)^{0.067} \times 10^{-6.07}[Fe^{3+}]^{0.93}[Fe^{2+}]^{-0.4} \quad (6)$$

Fig. 2(B) shows the degradation kinetics of *p*-NP in the pyrite heterogeneous Fenton reaction using 7 different pyrite dosages varying from 0.1 to 2.0 g L^{-1} at pH 4. The degradation kinetics of *p*-NP at different pyrite dosages was properly fitted with pseudo-first-order rate equation. The degradation kinetics of *p*-NP was enhanced as pyrite dosage increased. The estimated rate constant of *p*-NP increased by 17.9 times from 0.0489 to 0.8736 min^{-1} as pyrite dosage increased by 20 times from 0.1 to 2.0 g L^{-1}. The inset of Fig. 2(B) shows a linear regression fit which was used to explain the proportional increase of kinetic rate constants for pyrite dosage, of which slope under pyrite dosage was calculated to be 0.4464 L g^{-1} min^{-1}, implying the degradation of *p*-NP was significantly impacted by the content of pyrite, which can be explained by the increasing accessible active sites.[3] It was reported when a mass ratio of 1000/1.11 (micro-pyrite/H_2O_2) was employed, chloramphenicol removal showed a decline due to scavenging effects on ${}^{\bullet}OH$.[34] However, owing to a smaller mass ratio (1000/51) used, the reduction of kinetic rate constants was not observed in our study.

The purpose of adding H_2O_2 in Fenton process is to generate ${}^{\bullet}OH$, while excessive H_2O_2 consume ${}^{\bullet}OH$.[13] Tus the effect of H_2O_2 concentrations on the degradation kinetics of *p*-NP is presented in Fig. 2(C). The degradation kinetics of *p*-NP at an H_2O_2 concentration range of 1–10 mM can be properly fitted with a pseudo-first-order rate equation. The estimated rate constant of *p*-NP increased by 14.6 times from 0.0404 to 0.5890 min^{-1} as H_2O_2 concentration increased by 10 times from 1 to 10 mM. A linear regression fit, showing in the inset of Fig. 2(C), was employed to interpret the augment of kinetic rate constants in respect of H_2O_2 concentration, the slope of which was calculated to be 0.061 L mol^{-1} min^{-1}. It can be concluded that the degradation kinetics of *p*-NP was highly influenced by H_2O_2 concentration. This tendency was in agreement with the previous studies,[18] which proposed once an appropriate dosage of iron-based-catalyst was employed, the increase of H_2O_2 concentration could enhance the degradation of organic pollutants due to improved ${}^{\bullet}OH$ formation. 100 mg L^{-1} of *p*-NP was completely degraded within 30 min while 3 mM H_2O_2 was used. The degradation time was reduced to 10 min while using 10 mM H_2O_2. This was foreseen cause 10 mM H_2O_2 was slightly exceeded the amount required for complete mineralization of 100 mg L^{-1} *p*-NP. However, the scavenging of ${}^{\bullet}OH$ caused by the increase of H_2O_2 concentration (eqn (7))[13] did not seem to be

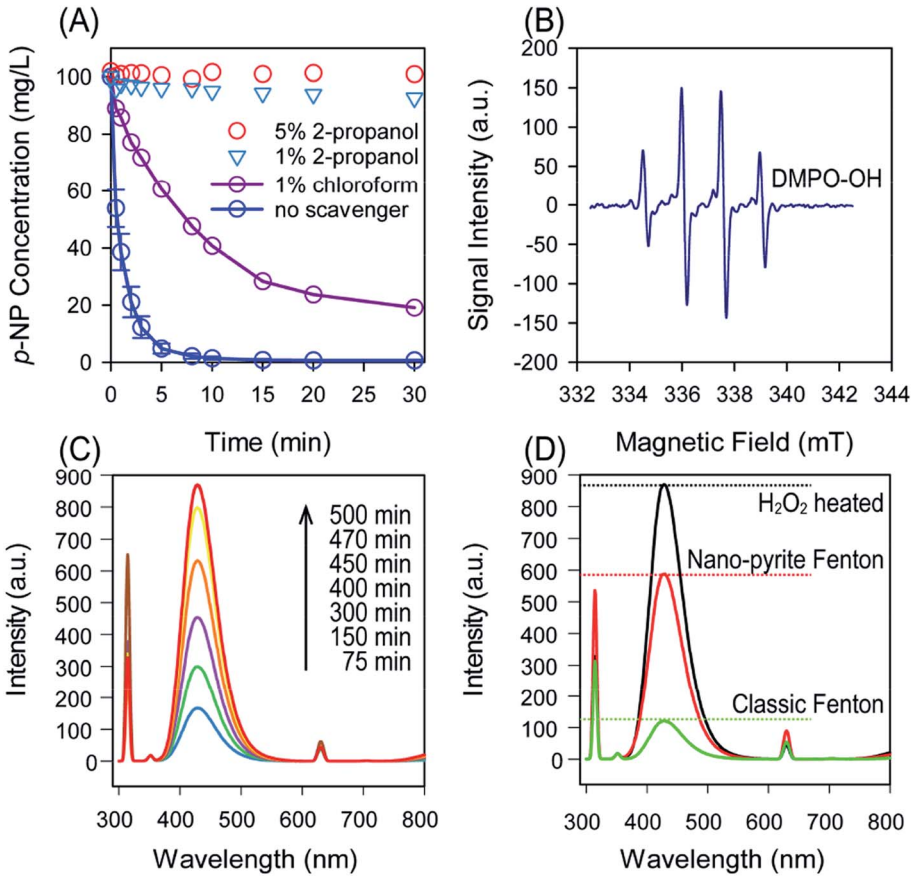

Fig. 3 (A) Effects of scavengers on the degradation of *p*-NP. (B) Electron spin resonance spectra for DMPO-OH in the pyrite Fenton system. (C) Fluoresce intensity of a mixture of H_2O_2 (3 mM) and benzoic acid (diluted for 20 times) with the increase of time heated at 90 °C. (D) Fluoresce intensity of hydroxybenzoic acid (diluted 20 times) generated in different systems.

Open Access Article. Published on 22 April 2020. Downloaded on 10/31/2025 4:51:06 PM.
This article is licensed under a Creative Commons Attribution-NonCommercial 3.0 Unported Licence.

a significant step during the reaction, which could lead to the deceleration of *p*-NP degradation kinetics and was due to the low H_2O_2 concentration (<10 mM) employed.

$$H_2O_2 + {}^{\bullet}OH \rightarrow {}^{\bullet}OOH + H_2O \quad (7)$$

The effect of initial pH on the degradation kinetics of *p*-NP in pyrite heterogeneous Fenton reaction is shown in Fig. 2(D). As the initial pH increased from 4 to 10, the degradation kinetics decelerated. The best degradation of *p*-NP was at pH 4, the kinetic rate constant of which (0.3771 min^{-1}) was 2.03, 1.32, and 1.25 ($p < 0.001$) times higher than that of pH 1 (0.1858 min^{-1}), pH 7 (0.2849 min^{-1}), and pH 10 (0.3005 min^{-1}), respectively. This decreasing rate constants with increasing initial pH can be explained by the fact that more H_2O_2 was decomposed through a non-radical way with the form of H_2O and O_2, rather than through a radical way to generate $^{\bullet}OH$ at higher pH.[3] $^{\bullet}OH$ has a smaller oxidation potential at basic environment than that of acidic condition (eqn (8) and (9)),[35] leading to the observed reduction in kinetic rate constants.

$$^{\bullet}OH + e^- + H^+ \rightarrow H_2O \quad (8)$$

$$^{\bullet}OH + e^- \rightarrow OH^- \quad (9)$$

In conventional Fenton, the optimal pH was reported to be between 3 to 6, for pH lower than 3 or higher than 6, a decrease of degradation kinetics and early termination occurred due to the precipitation of $Fe(OH)_3$. pH in the pyrite Fenton reaction decreased and reached an equilibrium point by releasing iron and hydrogen (eqn (1), (2) and (4)), providing an optimal pH for the Fenton reaction.[36] Hence, although the kinetic rate constants varied, proximately all *p*-NP were degraded within 30 min, except for pH 1. The isoelectric point (IEP) value of pyrite varies from 1.4 to 1.7,[37] thus the pyrite is presumable positively charged under a lower pH value (*i.e.* pH 1). The pK_a value of *p*-NP was reported to be 7.08 at 22 °C[3] which meant that *p*-NP is positively charged under acid conditions. Therefore, the adsorption of *p*-NP onto the pyrite surface can be inhibited at pH 1 due to the electronic repulsion, which slows down the degradation of *p*-NP correspondingly.

Numerous studies pointed out that the pH utilized in Fenton cannot be increased without any limitation due to possible hydrolysis and precipitation of metal ions.[4] Because of the narrow pH range classic Fenton required, a prior pH adjustment process is always needed. While in nano-pyrite Fenton process, the pH drops very quickly to around 3.5 within 10 s once nano-pyrite was added into water (Fig. S2†), due to pyrite oxidation by dissolved oxygen, an additional pH adjustment can therefore be eliminated.

3.3 Determination of free radicals

The predominant radicals for pollutants oxidation in pyrite Fenton-like system were inconsistent, it was reported that $^{\bullet}OH$ is the main radical driving the oxidation of TCE, and the degradation of carbon tetrachloride was dominated by $^{\bullet}O_2^{2-}$.[38] To determine the primary radicals responsible for *p*-NP degradation, specific scavenging experiments were conducted (Fig. 3(A)). The results showed that the degradation of *p*-NP was significantly inhibited by the addition of iso-propanol. The degradation of *p*-NP was almost inhibited completely even when 1% (v/v) iso-propanol was employed. Although the degradation was also suppressed when adding 1% (v/v) chloroform, this is because chloroform could also react with $^{\bullet}OH$, though a lower rate constant was existed compared to that of iso-propanol. Additionally, the ESR revealed that $^{\bullet}OH$ was the predominant radicals (Fig. 3(B)). It was then confirmed that $^{\bullet}OH$ was the dominant reactive species responsible for *p*-NP degradation in nano-pyrite Fenton.

The yield of $^{\bullet}OH$ was measured by recording the fluorescence intensity of hydroxybenzoic acid generated from the capture of $^{\bullet}OH$ by benzoic acid (Fig. 3(C) and (D)).[39] Compared with classic Fenton, nano-pyrite Fenton exhibited enhanced fluorescence signal (Fig. 3(D)). The conversion efficiency of H_2O_2 into $^{\bullet}OH$ was an important index to characteristic Fenton. By employing the heating method,[5] the conversion efficiency was calculated to be 67.55% in nano-pyrite Fenton, which was much higher than that of conventional Fenton (13.90%).

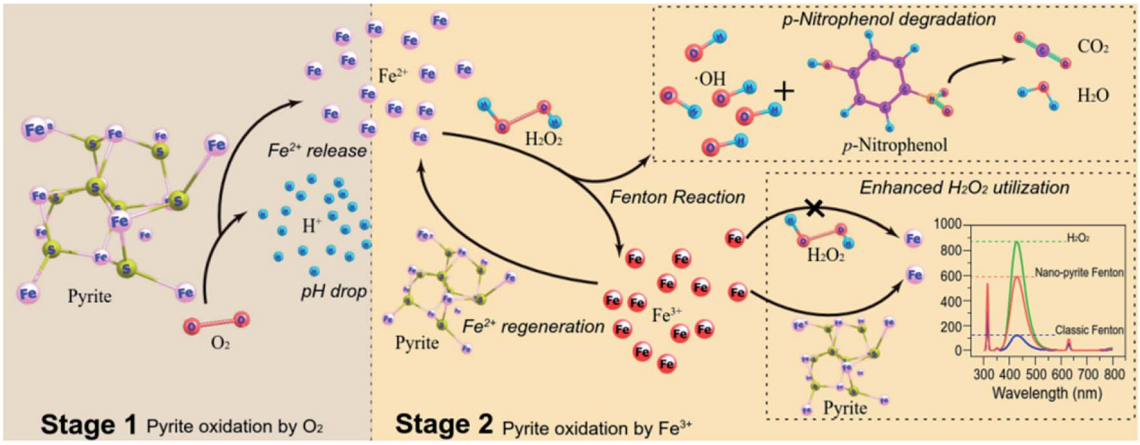

Fig. 4 Schematic illustration for the possible $^{\bullet}OH$ generation mechanism in nano-pyrite Fenton system.

Open Access Article. Published on 22 April 2020. Downloaded on 10/31/2025 4:51:06 PM.
This article is licensed under a Creative Commons Attribution-NonCommercial 3.0 Unported Licence.

3.4 Mechanism investigation

Fig. 4 illustrated our proposed mechanism of nano-pyrite Fenton. The first step is the oxidation of nano-pyrite by dissolved oxygen (eqn (1)), releasing H^+ and Fe^{2+}, which resulted in an acidic and Fe^{2+} rich environment. Once adding H_2O_2, the reaction between released Fe^{2+} (eqn (2)) and H_2O_2 generates massive $^{\bullet}OH$ attacking pollutants (eqn (3)). The produced Fe^{3+} then react rapidly with nano-pyrite (eqn (4)), rather than H_2O_2 (eqn (5)), with the regeneration of aqueous Fe^{2+} as a result. By this means a continuous $^{\bullet}OH$ production through homogeneous Fe^{2+} catalyzed Fenton is promised.

To confirm the proposed mechanism, we first examine the role of surface catalysis by conducting experiments utilizing 1,10-phenanthroline and pH adjustment, since surface activation and continuous release of Fe^{2+} were regarded as the main factors contributing to enhanced $^{\bullet}OH$ generation in micro-pyrite Fenton.[15,17] 1,10-Phenanthroline could reduce the concentration of aqueous Fe^{2+},[40] leading to a restrained aqueous reaction, the direct activation of H_2O_2 by nano-pyrite surface for $^{\bullet}OH$ generation was not suppressed. Inhibition of *p*-NP degradation was observed in the presence of 1 mM 1,10-phenanthroline (Fig. 5(D)). Thus, the restraint effect by 1,10-phenanthroline on *p*-NP degradation indicated that $^{\bullet}OH$ was generated more in homogeneous reaction than heterogeneous reaction. To provide further evidence for the homogeneous process, additional experiments were conducted employing 100 mM HPO_4^{2-} to maintain an alkaline environment. As the consequence of low solubility of Fe^{3+} in basic condition, the conversion of H_2O_2 into $^{\bullet}OH$ by Fe^{2+} generated through Fe^{3+} reduction can be negligible. The significant negative effect of HPO_4^{2-} (100 mM) on micro-pyrite Fenton reaction was observed previously, which was explained by the strong pH adjustment effect of HPO_4^{2-}.[25] Less than 25% of the *p*-NP was degraded within 30 min (Fig. 5(D)), confirming the proposed homogeneous reaction pathway again.

With the importance of aqueous iron in homogeneous Fenton, we then investigated the variation of aqueous iron species in nano-pyrite Fenton (Fig. 5(A)). Once nano-pyrite was added, a quick increment of aqueous total iron concentration to 5 mg L^{-1} was observed, it kept increase ongoingly to 6 mg L^{-1} in the first 3 min after reaction was initiated and remained very slow (<6.5 mg L^{-1}) as the reaction proceeded. The variation of Fe^{2+} and Fe^{3+} concentrations seemed more complex. The aqueous total iron was composed all by ferrous ion before H_2O_2 addition. Once Fenton reaction initiated, a dramatical ferrous concentration decrease and ferric concentration increase was observed in the early stage. Then ferric concentration arises ongoingly and turned to decrease after 5 min, while ferrous concentration kept an augment trend. However, once adding H_2O_2 into *p*-NP solutions containing $FeSO_4$, aqueous Fe^{2+}

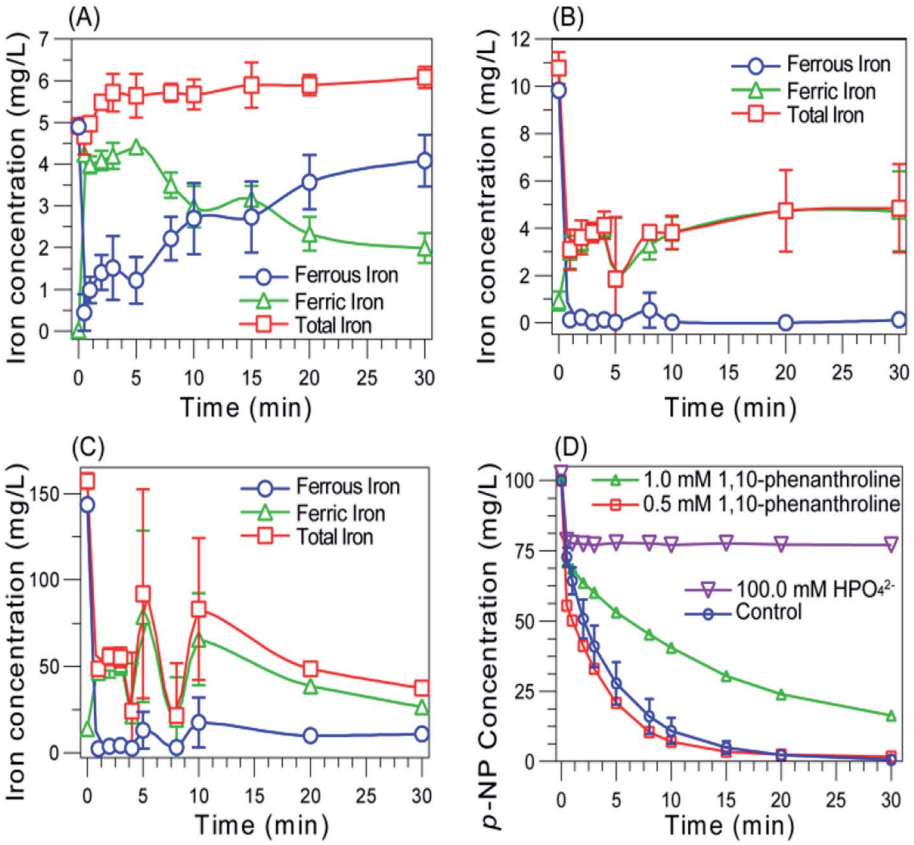

Fig. 5 The changes of Fe species in pyrite nanoparticles (A), 10 mg L^{-1} soluble Fe^{2+} (B), and 150 mg L^{-1} soluble Fe^{2+} (C) catalyzed Fenton system, and *p*-NP degradation under Fe^{2+} restricted conditions (D). Experimental boundary conditions: $[p\text{-NP}]_0 = 100$ mg L^{-1}, pyrite dosage = 0.30 g L^{-1}, $[H_2O_2]_0 = 3.0$ mM, pH = 4, and temperature = 25 ± 0.5 °C.

Open Access Article. Published on 22 April 2020. Downloaded on 10/31/2025 4:51:06 PM.
This article is licensed under a Creative Commons Attribution-NonCommercial 3.0 Unported Licence.

transformed into Fe^{3+} immediately and kept a very low level thereafter (Fig. 5(B) and (C)).

Due to the high abundance of Fe^{3+} among aqueous species, a Fe^{3+} catalyzed Fenton-like reaction, which produces $^{\bullet}OOH$ following (eqn (5)), became the dominant reaction in these systems. Although the Fe^{3+}/Fe^{2+} cycle was also observed in micro-pyrite Fenton,[38] the low regeneration rate was not reasonable to improve $^{\bullet}OH$ generation. It was concluded that an enhanced Fe^{3+}/Fe^{2+} cycle based on nano-pyrite promoted the homogeneous Fenton generating $^{\bullet}OH$ continuously, and supported the overall *p*-NP degradation.

The regeneration of Fe^{2+} through the reduction of Fe^{3+} by H_2O_2 (eqn (5)) is the rate-limiting step in the Haber–Wiess cycle. Thus, any approach promoting the regeneration of Fe^{2+} would accelerate the decomposition of H_2O_2 and the formation of $^{\bullet}OH$. In addition to the supplement of much more active sites, the much higher ferric reduction efficiency observed in nano-pyrite Fenton-like system than micro-pyrite Fenton system may be owing to (1) reduction of Fe^{3+} to Fe^{2+} by intermediate products of *p*-NP degradation[41], (2) release Fe^{2+} through the oxidation of nano-pyrite by Fe^{3+} (eqn (4)).

A larger degradation rate of *p*-NP by pyrite Fenton reaction than classic Fenton reaction was observed (Fig. 2), suggesting the reduction of Fe^{3+} due to the electron donor effect of intermediates (*i.e.* the first hypothesis) was the case. Despite a quick rise of total aqueous iron concentration in the very early stage of reaction, a slight increase was observed from Fig. 5(A), which could be related to the oxidation of nano-pyrite by Fe^{3+} (eqn (4)). The results obtained above suggested that the high efficiency of nano-pyrite was mainly due to the sufficient Fe^{2+} supply from the autocatalytic oxidation of nano-pyrite by Fe^{3+}. The adsorption of Fe^{3+} onto nano-pyrite surface and redistribution of regenerated Fe^{2+} into aqueous solution was favored due to the poor water solubility of Fe^{3+} and excellent water solubility of Fe^{2+},[5] making this autocatalytic process perform much easier.

Owing to its significant importance as the main contributor to acid mine drainage problem,[42] the surface oxidation and dissolution processes of pyrite, which was controlled mainly by Fe^{3+} (*i.e.* the autocatalytic oxidation process),[43] have been studied extensively in the past decades. Two electrochemical processes involving electron transfer from surface Fe^{2+} to aqueous Fe^{3+} (cathodic reaction) and sulfur oxidation (anode reaction) present in this oxidation reaction.[27] Although the elementary steps of this redox reaction is quite complex and the key controls of mechanisms remain poorly understood, it was confirmed that seven electrons, generating by the oxidation of S from S_2^{2-} to SO_4^{2-}, can be transferred through crystal pyrite to reduce aqueous Fe^{3+}.[27] A wide range of reactivity was observed using different pyrite samples.[44] It was pointed out that the size of pyrite affects the oxidation rate the most.[45] Thus, it was reasonably concluded that when the particle size comes to nanoscale with a much bigger SSA and more non-stoichiometric defect sites which was produced by the rupture of Fe–S and S–S bonds at pyrite surface during mechanical fracture process, the autocatalytic oxidation process was highly enhanced, suggesting the regeneration of Fe^{2+} by the reduction of Fe^{3+} on pyrite surface played a more important role in nano-pyrite Fenton-like system compared to micro-pyrite Fenton.

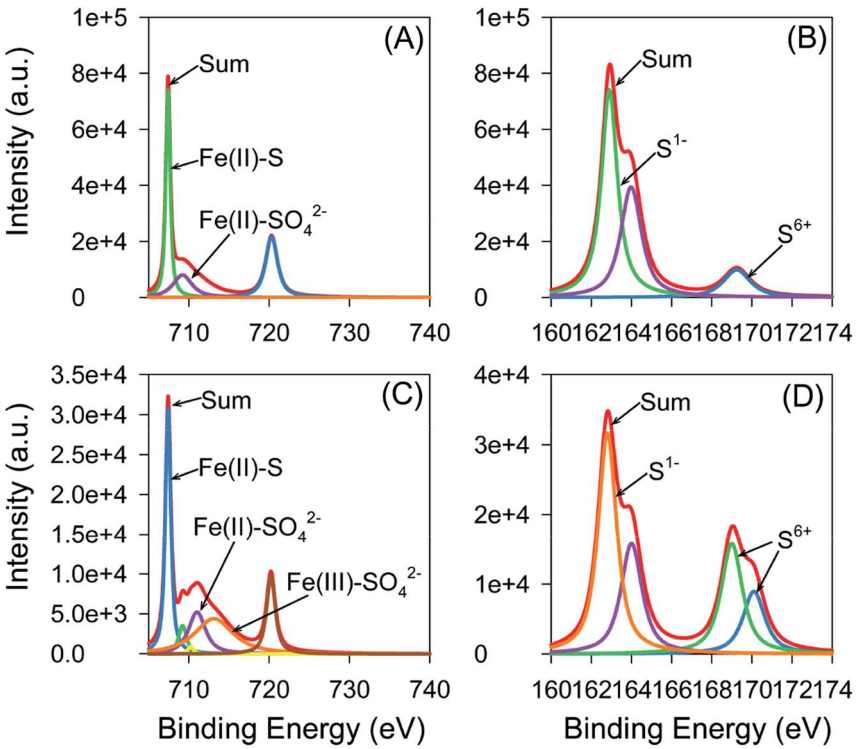

Fig. 6 XPS survey of Fe (2p) before (A) and after (B) reaction and S (2p) before (C) and after (D) reaction of the pyrite catalyst.

Open Access Article. Published on 22 April 2020. Downloaded on 10/31/2025 4:51:06 PM.
This article is licensed under a Creative Commons Attribution-NonCommercial 3.0 Unported Licence.

To further investigate the transformation of Fe and S on pyrite surface, the species of Fe and S were analyzed using XPS (Fig. 6). The binding energy (B.E.) peaks of Fe ($2p_{3/2}$) are located at 707.5, 711.0, 709.2, 713.1, and 710.2 eV, which corresponds to Fe(II)–S, Fe(II)–SO_4^{2-}, Fe(III)–S, Fe(III)–SO_4^{2-}, and Fe(III)–O, respectively.[46–48] The B.E. peaks of S (2p) are located at 162.8, 164, and 169.0/170.1 eV which stand for S_2^{2-}, S_n^{2-}, and SO_4^{2-}, respectively.[49–51] Fe(II)–S is the dominant Fe species with little Fe(III)–S and Fe(II)–SO_4^{2-}, and S_2^{2-} is the dominant S species with little SO_4^{2-}, observed at the surface of pyrite before the reaction. FeS_2 is the main component of cubic pyrite, and Fe(III)–S and Fe(II)–SO_4^{2-} were produced during the mechanic ball milling process and in humid air.[52] After reaction, a significant increase in peak intensity near 169.0 and 170.1 eV was observed from the S (2p) spectrum, while a slight rise in peak intensity near 711.0 and 713.1 eV was found from the Fe (2p) spectrum simultaneously, implying no big transformation of Fe happened during the reaction, while S species transformed from S(−I) to S(VI).

Despite the low catalytic efficiency caused by the slow reduction of Fe^{3+} to Fe^{2+} (eqn (5)), the catalytic capacity of classic Fenton reaction was also limited by this reduction process.[53] H_2O_2 acts as electron donor and was oxidized to O_2, thus a large amount of H_2O_2 was thus wasted. However, in pyrite Fenton system, this bottleneck of classic Fenton system was eliminated through the autocatalytic oxidation reaction of pyrite (eqn (4)). During this process, S atoms in pyrite were employed, replacing H_2O_2, as an electron donor. One electron can be transferred for Fe^{2+} regeneration consuming one H_2O_2 which was originally used for producing $^{\bullet}OH$ in classic Fenton system, during the transformation from S_2^{2-} to SO_4^{2-}, however, seven electrons could be provided to reduce Fe^{3+}.[27] By replacing H_2O_2 with S on pyrite surface as electron source, H_2O_2 was not consumed in Fe^{2+} regeneration but was used mainly for $^{\bullet}OH$ production, resulting in a highly increased stoichiometric efficiency (33%) compared to that of other catalysts (0.04–8.99%).[3,33]

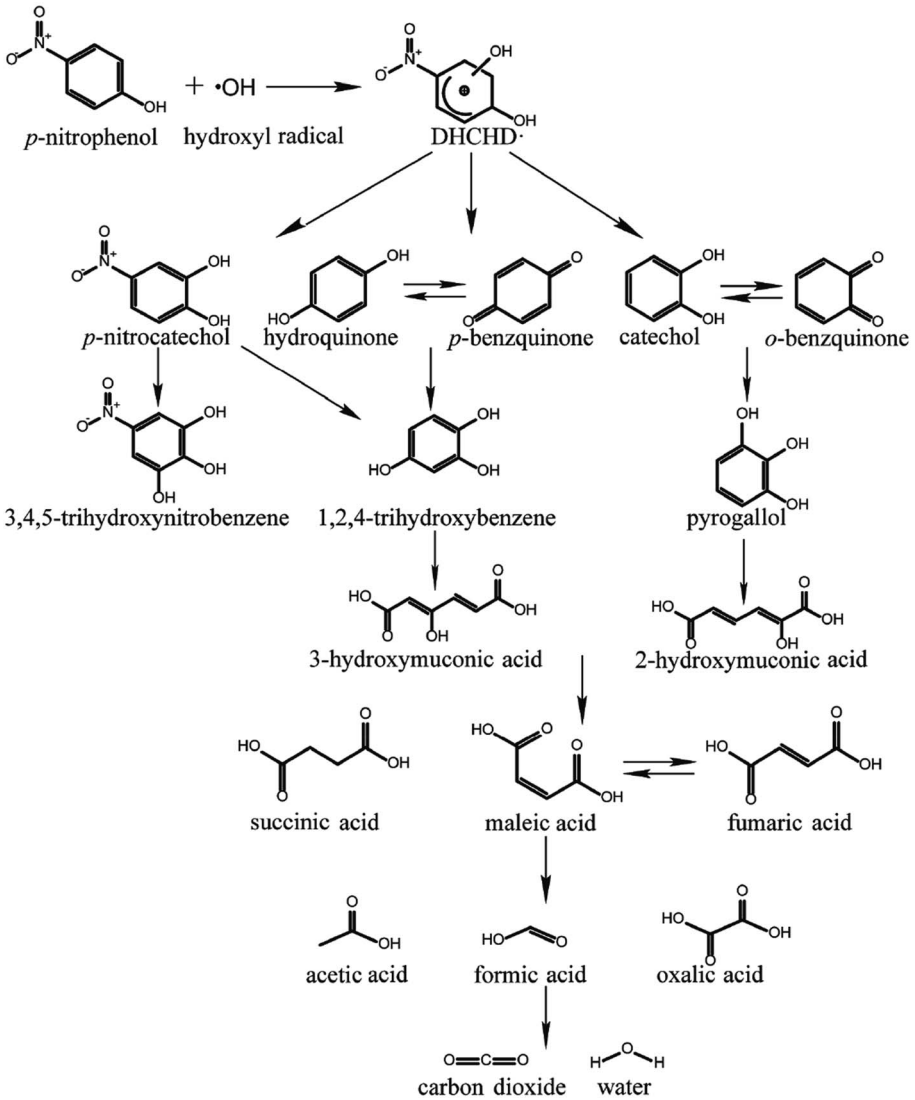

Fig. 7 Possible *p*-NP mineralization pathway in nano-pyrite Fenton system.

Open Access Article. Published on 22 April 2020. Downloaded on 10/31/2025 4:51:06 PM.
This article is licensed under a Creative Commons Attribution-NonCommercial 3.0 Unported Licence.

3.5 Mineralization pathway of *p*-NP

The mineralization products were identified by GC-MS. Nitrobenzene ($[M/H]^-$ *m*/*z* 123), hydroquinone ($[M/H]^-$ *m*/*z* 109), *p*-benzoquinone ($[M/H]^-$ *m*/*z* 107), *o*-benzoquinone ($[M/H]^-$ *m*/*z* 107), and 1,2,4-trihydroxybenzene ($[M/H]^-$ *m*/*z* 126) were detected. Based on the identified compounds, a plausible mineralization pathway of *p*-NP by pyrite Fenton process was proposed (Fig. 7) and interpreted detailly in ESI.†

3.6 Catalyst durability and scale-up experiment

To highlight the potential of nano-pyrite Fenton for industrial applications, catalyst durability, and scale-up experiments were designed. The durability test over 4 cycles was conducted for both nano-pyrite Fenton and classic Fenton system by adding 100 mg L^{-1} *p*-NP and 3 mM H_2O_2 continuously (Fig. S6†). And the experiment system was scaled up from 100 mL to 1.0 L. Although the degradation intermediates accumulated in the reaction solution due to the rather low H_2O_2 addition, it still showed a high *p*-NP removal efficiency (>80%) over 4 cycles. In the enlarged experiment system, nano-pyrite still showed an excellent catalytic reactivity, 100% *p*-NP removal was achieved within 5 min (Fig. S7†), which could be attributed to higher ferrous concentration in aqueous form.

4. Conclusion

The successful *p*-NP degradation under neutral initial pH was achieved by Fenton utilizing nano-pyrite produced by high energy planet ball milling as catalyst. The results showed that *p*-NP can be removed within 20 min at an initial *p*-NP concentration of 100 mg L^{-1}, nano-pyrite dosage of 0.30 g L^{-1}, and H_2O_2 concentration of 3 mM. Using nano-pyrite increased the $^{\bullet}OH$ conversion efficiency from 13.90% (conventional Fenton) to 67.55% by the high Fe^{2+} regeneration rate nano-pyrite supplied, leading to less H_2O_2 required. The major transformation products were generated through the attack of $^{\bullet}OH$ to the nitro-group and aromatic ring of *p*-NP. The limitations of classic Fenton, such as high cost and maintenance of the acidic environment, can be overcome by nano-pyrite Fenton. Therefore, this process can be considered as a promising technology for the remediation of *p*-NP and other refractory compounds contaminated water.

Conflicts of interest

There are no conflicts to declare.

Acknowledgements

The authors acknowledge financial support from Major Science and Technology Program for Water Pollution Control and Treatment (No. 2017ZX07202002), the National Natural Science Foundation of China (NSFC) (No. 51578519), and the Fundamental Research Funds for the Central Universities (No. 2652017189).

References

1 S. Wu, H. Li, X. Li, H. He and C. Yang, Performances and mechanisms of efficient degradation of atrazine using peroxymonosulfate and ferrate as oxidants, *Chem. Eng. J.*, 2018, **353**, 533–541.
2 S. Wu, Y. Lin, C. Yang, C. Du, Q. Teng, Y. Ma, *et al.*, Enhanced activation of peroxymonosulfte by $LaFeO_3$ perovskite supported on Al_2O_3 for degradation of organic pollutants, *Chemosphere*, 2019, **237**, 124478.
3 S.-P. Sun and A. T. Lemley, *p*-Nitrophenol degradation by a heterogeneous Fenton-like reaction on nano-magnetite: process optimization, kinetics, and degradation pathways, *J. Mol. Catal. A: Chem.*, 2011, **349**(1–2), 71–79.
4 N. Wang, T. Zheng, G. Zhang and P. Wang, A review on Fenton-like processes for organic wastewater treatment, *J. Environ. Chem. Eng.*, 2016, **4**(1), 762–787.
5 M. Xing, W. Xu, C. Dong, Y. Bai, J. Zeng, Y. Zhou, *et al.*, Metal Sulfides as Excellent Co-catalysts for H_2O_2 Decomposition in Advanced Oxidation Processes, *Chem*, 2018, **4**, 1–14.
6 Z. Yang, A. Yu, C. Shan, G. Gao and B. Pan, Enhanced Fe(III)-mediated Fenton oxidation of atrazine in the presence of functionalized multi-walled carbon nanotubes, *Water Res.*, 2018, **137**, 37–46.
7 S. Wu, H. Liu, Y. Lin, C. Yang, W. Lou, J. Sun, *et al.*, Insights into mechanisms of UV/ferrate oxidation for degradation of phenolic pollutants: role of superoxide radicals, *Chemosphere*, 2020, **244**, 125490.
8 N. Dulova, M. Trapido and A. Dulov, Catalytic degradation of picric acid by heterogeneous Fenton-based processes, *Environ. Technol.*, 2011, **32**(3–4), 439.
9 S. Keramidis and L. Mackert, Wastewater treatment with heterogeneous Fenton-type catalysts based on porous materials, *J. Mater. Chem.*, 2010, **20**(41), 9002–9017.
10 M. C. Pereira, L. C. A. Oliveira and E. Murad, Iron oxide catalysts: Fenton and Fentonlike reactions – a review, *Clay Miner.*, 2012, **47**(3), 285–302.
11 S. Ammar, M. A. Oturan, L. Labiadh, A. Guersalli, R. Abdelhedi, N. Oturan, *et al.*, Degradation of tyrosol by a novel electro-Fenton process using pyrite as heterogeneous source of iron catalyst, *Water Res.*, 2015, **74**, 77–87.
12 R. Matta, K. Hanna and S. Chiron, Fenton-like oxidation of 2,4,6-trinitrotoluene using different iron minerals, *Sci. Total Environ.*, 2007, **385**(1), 242–251.
13 S. Bae, D. Kim and W. Lee, Degradation of diclofenac by pyrite catalyzed Fenton oxidation, *Appl. Catal., B*, 2013, **134–135**, 93–102.
14 Y. Zhang, K. Zhang, C. Dai, X. Zhou and H. Si, An enhanced Fenton reaction catalyzed by natural heterogeneous pyrite for nitrobenzene degradation in an aqueous solution, *Chem. Eng. J.*, 2014, **244**, 438–445.
15 H. Che, S. Bae and W. Lee, Degradation of trichloroethylene by Fenton reaction in pyrite suspension, *J. Hazard. Mater.*, 2011, **185**(2), 1355–1361.

Open Access Article. Published on 22 April 2020. Downloaded on 10/31/2025 4:51:06 PM.
This article is licensed under a Creative Commons Attribution-NonCommercial 3.0 Unported Licence.

16 R. Matta, K. Hanna, T. Kone and S. Chiron, Oxidation of 2,4,6-trinitrotoluene in the presence of different iron-bearing minerals at neutral pH, *Chem. Eng. J.*, 2008, **144**(3), 453–458.

17 K. Choi, S. Bae and W. Lee, Degradation of pyrene in cetylpyridinium chloride-aided soil washing wastewater by pyrite Fenton reaction, *Chem. Eng. J.*, 2014, **249**, 34–41.

18 S. Fathinia, M. Fathinia, A. A. Rahmani and A. Khataee, Preparation of natural pyrite nanoparticles by high energy planetary ball milling as a nanocatalyst for heterogeneous Fenton process, *Appl. Surf. Sci.*, 2015, **327**, 190–200.

19 K. Choi, S. Bae and W. Lee, Degradation of off-gas toluene in continuous pyrite Fenton system, *J. Hazard. Mater.*, 2014, **280**(suppl. C), 31–37.

20 J. Meijide, E. Rosales, M. Pazos and M. A. Sanromán, *p*-Nitrophenol degradation by electro-Fenton process: pathway, kinetic model and optimization using central composite design, *Chemosphere*, 2017, **185**, 726–736.

21 A. Zhang, N. Wang, J. Zhou, P. Jiang and G. Liu, Heterogeneous Fenton-like catalytic removal of *p*-nitrophenol in water using acid-activated fly ash, *J. Hazard. Mater.*, 2012, **201–202**(suppl. C), 68–73.

22 J. Cui, T. Qian, Q. Ding and F. Ding, Adsorption of Cr^{6+}, Cd^{2+} and Pb^{2+} from aqueous solutions by nanoscale pyrite, *Chin. J. Environ. Eng.*, 2016, **10**(12), 7103–7108.

23 K. Liu, *The study on the kinetics of the preparation of iron sulfides particles by mechano-chemistry method in nonaqueous systems [Internet] [Master]*, Central South University, Changsha, 2008, available from http://d.wanfangdata.com.cn/Thesis/Y1324354.

24 Y. Bai, J. Yeom, M. Yang, S.-H. Cha, K. Sun and N. A. Kotov, Universal Synthesis of Single-Phase Pyrite FeS_2 Nanoparticles, Nanowires, and Nanosheets, *J. Phys. Chem. C*, 2013, **117**(6), 2567–2573.

25 Z.-H. Diao, J.-J. Liu, Y.-X. Hu, L.-J. Kong, D. Jiang and X.-R. Xu, Comparative study of rhodamine B degradation by the systems pyrite/H_2O_2 and pyrite/persulfate: reactivity, stability, products and mechanism, *Sep. Purif. Technol.*, 2017, **184**(suppl. C), 374–383.

26 Y. Xian, Q. Nie, S. Wen, J. Liu and J. Deng, Investigation of pyrite surface state by DFT and AFM, *J. Cent. South Univ.*, 2015, **22**(7), 2508–2514.

27 J. D. Rimstidt and D. J. Vaughan, Pyrite oxidation: a state-of-the-art assessment of the reaction mechanism, *Geochim. Cosmochim. Acta*, 2003, **67**(5), 873–880.

28 Z.-H. Diao, X.-R. Xu, D. Jiang, G. Li, J.-J. Liu, L.-J. Kong, *et al.*, Enhanced catalytic degradation of ciprofloxacin with FeS_2/SiO_2 microspheres as heterogeneous Fenton catalyst: kinetics, reaction pathways and mechanism, *J. Hazard. Mater.*, 2017, **327**, 108–115.

29 M. A. Williamson and J. D. Rimstidt, The kinetics and electrochemical rate-determining step of aqueous pyrite oxidation, *Geochim. Cosmochim. Acta*, 1994, **58**, 5443–5454.

30 M. A. Mckibben and H. L. Barnes, Oxidation of pyrite in low temperature acidic solutions: rate laws and surface textures, *Geochim. Cosmochim. Acta*, 1986, **50**(7), 1509–1520.

31 A. L.-T. Pham, C. Lee, F. M. Doyle and D. L. Sedlak, A Silica-Supported Iron Oxide Catalyst Capable of Activating Hydrogen Peroxide at Neutral pH Values, *Environ. Sci. Technol.*, 2009, **43**(23), 8930–8935.

32 W. Huang and J. Ruan, Degradation of 4-nitrophenol using zero value iron metal of Fenton process facilitated by microwave irradiation, in *E-Product E-Service and E-Entertainment (ICEEE), 2010 International Conference on [Internet]*, IEEE, 2010, pp. 1–5, available from http://ieeexplore.ieee.org/abstract/document/5660573/.

33 H. Ren, Y. Su, X. Han and R. Zhou, Synthesis and characterization of saponin-modified Fe_3O_4 nanoparticles as heterogeneous Fenton-catalyst with enhanced degradation of *p*-nitrophenol, *J. Chem. Technol. Biotechnol.*, 2017, **92**(6), 1421–1427.

34 D. Wu, Y. Chen, Z. Zhang, Y. Feng, Y. Liu, J. Fan, *et al.*, Enhanced oxidation of chloramphenicol by GLDA-driven pyrite induced heterogeneous Fenton-like reactions at alkaline condition, *Chem. Eng. J.*, 2016, **294**, 49–57.

35 G. P. Anipsitakis and D. D. Dionysiou, Degradation of Organic Contaminants in Water with Sulfate Radicals Generated by the Conjunction of Peroxymonosulfate with Cobalt, *Environ. Sci. Technol.*, 2003, **37**(20), 4790–4797.

36 Y. Zhang, K. Zhang, C. Dai and X. Zhou, Performance and mechanism of pyrite for nitrobenzene removal in aqueous solution, *Chem. Eng. Sci.*, 2014, **111**, 135–141.

37 R. Murphy and D. R. Strongin, Surface reactivity of pyrite and related sulfides, *Surf. Sci. Rep.*, 2009, **64**(1), 1–45.

38 H. Che and W. Lee, Selective redox degradation of chlorinated aliphatic compounds by Fenton reaction in pyrite suspension, *Chemosphere*, 2011, **82**(8), 1103–1108.

39 K. Ishibashi, A. Fujishima, T. Watanabe and K. Hashimoto, Detection of active oxidative species in TiO_2 photocatalysis using the fluorescence technique, *Electrochem. Commun.*, 2000, **2**(3), 207–210.

40 J. Du, W. Guo, H. Wang, R. Yin, H. Zheng, X. Feng, *et al.*, Hydroxyl radical dominated degradation of aquatic sulfamethoxazole by Fe^0/bisulfite/O_2: kinetics, mechanisms, and pathways, *Water Res.*, 2018, **138**, 323–332.

41 Y. Du, M. Zhou and L. Lei, Role of the intermediates in the degradation of phenolic compounds by Fenton-like process, *J. Hazard. Mater.*, 2006, **136**(3), 859–865.

42 D. Wu, Y. Chen, Y. Zhang, Y. Feng and K. Shih, Ferric iron enhanced chloramphenicol oxidation in pyrite (FeS_2) induced Fenton-like reactions, *Sep. Purif. Technol.*, 2015, **154**, 60–67.

43 M. Fehr, *The Threshold Target Approach to Waste Management in Emerging Economies: Pragmatic, Realistic, Appropriate*, INTECH Open Access Publisher, 2010.

44 F. Howie, *The Care and Conservation of Geological Material: Minerals, Rocks, Meteorites, and Lunar Finds*, Butterworth-Heinemann, 1992, p. 172.

45 F. T. Caruccio, *The Ecology of Resource Degradation and Renewal: Symposium Proceedings*, ed. M. J. Chadwick and G. T. Goodman, Blackwell Science Ltd, Oxford, 1975, p. 460.

46 H. W. Nesbitt and I. J. Muir, Oxidation states and speciation of secondary products on pyrite and arsenopyrite reacted

Open Access Article. Published on 22 April 2020. Downloaded on 10/31/2025 4:51:06 PM.
This article is licensed under a Creative Commons Attribution-NonCommercial 3.0 Unported Licence.

with mine waste waters and air, *Mineral. Petrol.*, 1998, **62**(1–2), 123–144.

47 B. J. Richardson, L. Zhu and Q. Yu, Inverted hybrid solar cells based on pyrite FeS_2 nanocrystals in P3HT:PCBM with enhanced photocurrent and air-stability, *Sol. Energy Mater. Sol. Cells*, 2013, **116**, 252–261.

48 T. Yamashita and P. Hayes, Analysis of XPS spectra of Fe^{2+} and Fe^{3+} ions in oxide materials, *Appl. Surf. Sci.*, 2008, **254**(8), 2441–2449.

49 M. Descostes, F. Mercier, N. Thromat, C. Beaucaire and M. Gautier-Soyer, Use of XPS in the determination of chemical environment and oxidation state of iron and sulfur samples: constitution of a data basis in binding energies for Fe and S reference compounds and applications to the evidence of surface species of an oxidized pyrite in a carbonate medium, *Appl. Surf. Sci.*, 2000, **165**(4), 288–302.

50 M. Mullet, S. Boursiquot, M. Abdelmoula, J.-M. Génin and J.-J. Ehrhardt, Surface chemistry and structural properties of mackinawite prepared by reaction of sulfide ions with metallic iron, *Geochim. Cosmochim. Acta*, 2002, **66**(5), 829–836.

51 S. Seefeld, M. Limpinsel, Y. Liu, N. Farhi, A. Weber, Y. Zhang, *et al.*, Iron Pyrite Thin Films Synthesized from an $Fe(acac)_3$ Ink, *J. Am. Chem. Soc.*, 2013, **135**(11), 4412–4424.

52 L. Zhao, Y. Chen, Y. Liu, C. Luo and D. Wu, Enhanced degradation of chloramphenicol at alkaline conditions by S(−II) assisted heterogeneous Fenton-like reactions using pyrite, *Chemosphere*, 2017, **188**, 557–566.

53 L. Lyu and C. Hu, Heterogeneous Fenton Catalytic Water Treatment Technology and Mechanism, *Prog. Chem.*, 2017, **29**(9), 981–999.

 This journal is © The Royal Society of Chemistry 2020